J. Mater. Environ. Sci. 7 (8) (2016) 2897-2907 *Qachchachi et al.*
ISSN : 2028-2508
CODEN: JMESCN

Inhibitive Properties and Quantum Chemical Studies of (1-((1-benzyl-1H-1,2,3-triazol-4-yl)methyl)indoline-2,3-dione on Mild Steel Corrosion in Acidic Medium

F. -Z. Qachchachi[1,2], Y. Kandri Rodi[1], H. Elmsellem[3*], H. Steli[6], A. Haoudi[2], A. Mazzah[4], Y. Ouzidan[1], N. K. Sebbar[5], E. M. Essassi[5]

[1] *Laboratoire de Chimie Organique Appliquée, Université Sidi Mohamed Ben Abdallah, Faculté des Sciences et Techniques, Route d'Immouzzer, BP 2202 Fès, Morocco,*

[2]*Laboratoire de Chimie Appliquée, Université Sidi Mohamed Ben Abdallah, Faculté des Sciences et Techniques, Route d'Immouzzer, BP 2202 Fès, Morocco,*

[3] *Laboratoire de chimie analytique appliquée, matériaux et environnement (LC2AME), Faculté des Sciences, B.P. 717, 60000 Oujda, Morocco,*

[4] *Laboratoire de Spectrochimie Infra-rouge et Raman UMR8516, Universite des Sciences et Techniques de Lille, 59655 Villeneuve d'Ascq Cedex, France,*

[5]*Laboratoire de Chimie Organique Hétérocyclique, URAC 21, Pôle de Compétences Pharmacochimie, Mohammed V University, Faculté des Sciences, Av. Ibn Battouta, BP 1014 Rabat, Morocco.*

[6]*Laboratoire mécanique & énergétique, Faculté des Sciences, Université Mohammed Premier, Oujda, Maroc*

Received 17 Mar 2016, Revised 25 June 2016, Accepted 30 June 2016
**Corresponding author. E-mail: h.elmsellem@yahoo.fr, youssef_kandri_rodi@yahoo.fr; Tél : +212670923431*

Abstract
The inhibitory effect of 1-(1-benzyl-1H-1,2,3-triazol-4-yl)methyl)indoline-2,3-dione (P2) on the corrosion behaviour of mild steel in 1 M HCl, at (308 ± 1)K was studied by gravimetric, electrochemical impedance spectroscopy and DFT measurements. The effect of inhibitor concentration on the corrosion rate, surface coverage and inhibition efficiency is investigated. The results obtained show that P2 exerts a strong inhibiting effect on mild steel corrosion.

Keywords: Mild steel, 1H-indole-2,3-dione, EIS, Corrosion, Weight loss, EIS, DFT.

1. Introduction

Isatin (1H-indole-2,3-dione) derivatives are synthetically versatile substrates, used for the synthesis of a large variety of heterocyclic compounds, such as indoles and quinolines, and as raw material for drug synthesis[1–6] . The general process utilizes the effective method for synthesis of isatin from indole is bromination and oxidation with an N-bromosuccinimide- dimethyl sulfoxide reagent. The nitration of isatin at C-5 takes place by using KNO_3, con. H_2SO_4 [7–11].The pharmacological and biological properties of isatin derivatives include a range of actions in the brain and offer protection against certain types of infections. They possess anxiogenic, sedative, anticonvulsant activities and act as a potent antagonists on atrial natriuretic peptide receptors in vitro[12–17]. Due to the importance of heterocyclic systems containing triazole ring. a novel 1,2,3-triazolylmethyl-indoline-2,3-dione derivative has been synthesized employing both 1,3-dipolar cycloaddition and the click chemistry approach.
The present study aimed to test new compound namely 1-(1-benzyl-1H-1,2,3-triazol-4-yl)methyl)indoline-2,3-dione: (P2) (Figure 1) on the corrosion of mild steel in 1 M hydrochloric acid solution.

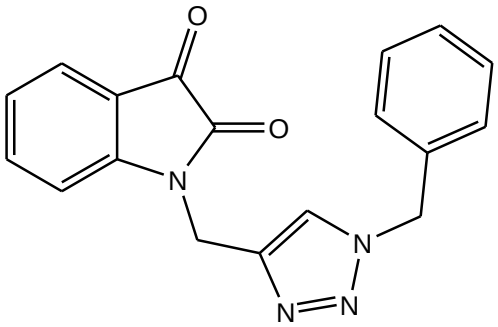

Figure 1: 1-(1-benzyl-1H-1,2,3-triazol-4-yl)methyl)indoline-2,3-dione [18] (P2)

2. Experimental

2.1. Synthesis of inhibitor

To a solution of 2.4 mmol of 1-(prop-2-ynyl)indoline-2,3-dione and (4.1 mmol) 1-(azido- methyl)benzene in 20 mL of ethanol were added at room temperature 0.5 mmol of $CuSO_4$ and 1 mmol of sodium ascorbate dissolved in 7 mL of distilled water. The mixture was stirred for 24 h and the reaction was monitored by TLC. After filtration of the salts and concentration of the solution in reduced pressure, the product obtained was purified by column chromatography on silica gel (eluent:ethyl acetate/hexane (3/1)) (**Scheme 1**):

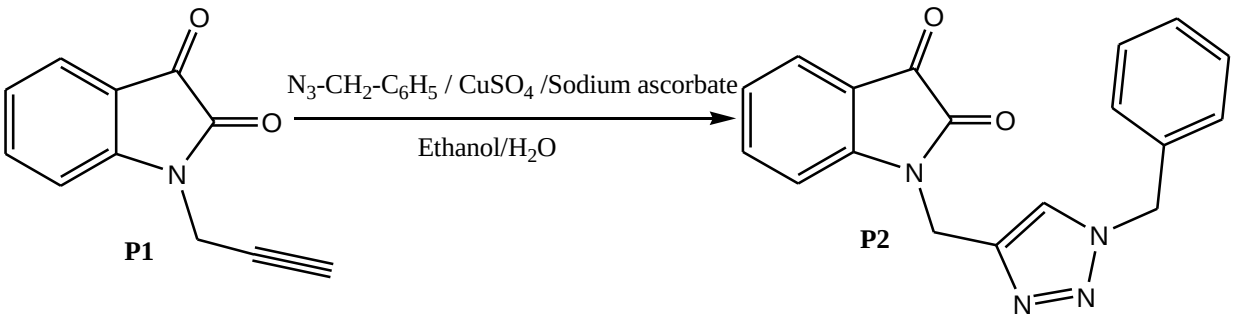

Scheme 2: Synthesis of 1-(1-benzyl-1H-1,2,3-triazol-4-yl)methyl)indoline-2,3-dione(**P2**).

The analytical and spectroscopic data are conforming to the structure of compounds formed:
(P2): Yield: 81%**; MP =** 426-428 **K; NMR^{1}H ($CDCl_3$-d6) δppm:** 5.498(s, 2H, CH_2benz); 4.9(s, 2H, CH_2-N); 7.101(s, 1H, CHtriazo); 7.630-7.103(m, 9H, CHarom). **NMR^{13}C ($CDCl_3$-d6) δppm:** 150.21, 157.92(C=O); 140.2, 133.97, 117.52, 117.02(Cq); 138.61(Ctriazo); 138.61, 129.50, 129.24, 129.02, 125.32, 124.02, 122.83, 121.17, 111.55, 111.54 (Carom); 54.45, 35.39(CH_2).

2.2. Materials

The steel used in this study is a mild steel with a chemical composition 0.09 wt. % P; 0.38 wt. % Si; 0.01 wt. % Al; 0.05 wt. % Mn; 0.21 wt. % C; 0.05 wt. % S and the remainder iron (Fe).

2.2.1. Preparation of Solutions

The aggressive solutions of 1.0 M HCl were prepared by dilution of analytical grade 37% HCl with distilled water. Inhibitor were dissolved in acid solution at the required concentrations (in mol/l) (volume of inhibitor/volume of HCl), and the solution in the absence of inhibitor was taken as blank for comparison purposes. The test solutions were freshly prepared before each experiment by adding P2 to the corrosive solution. The concentrations of P2 were 10^{-3} to 10^{-6} M.

2.2.2. Gravimetric Study

Gravimetric experiments were performed according to the standard methods [19], the carbon steel specimens (1.5 cm × 1.5 cm × 0.05 cm) were abraded with a series of emery papers SiC (120, 600, and 1200 grades) and

then washed with distilled water and acetone. After weighing accurately, the specimens were immersed in a 100 mL of 1.0 M HCl solution with and without addition of different concentrations of inhibitor P2.
All the aggressive acid solutions were open to air. After 6 hours of acid immersion, the specimens were taken out, washed, dried, and weighed accurately. In order to get good reproducibility, all measurements were performed few times and average values were reported.
The average weight loss was obtained. The corrosion rate (v) is calculated using the following equation:

$$v = \frac{w}{st} \qquad (\mathbf{1})$$

Where: W is the average weight loss, S the total area, and t is immersion time. With the corrosion rate calculated, the inhibition efficiency (E_w) is determined as follows:

$$Ew\ \% = \frac{V_0 - V}{V_0} X\ 100 \qquad (\mathbf{2})$$

Where: $\boldsymbol{v_0}$ and v are, respectively, the values of corrosion rate with and without inhibitor.

2.2.3. Electrochemical Measurements

The electrochemical measurements were carried out using Volta lab (Tacussel - Radiometer PGZ 100) potentiostat controlled by Tacussel corrosion analysis software model (Voltamaster 4) at static condition. The corrosion cell used had three electrodes. The reference electrode was a saturated calomel electrode (SCE). A platinum electrode was used as auxiliary electrode of surface area of 1 cm^2. The working electrode was carbon steel of the surface $1cm^2$. All potentials given in this study were referred to this reference electrode. The working electrode was immersed in the test solution for 30 minutes to establish a steady state open circuit potential (E_{ocp}). After measuring the E_{ocp}, the electrochemical measurements were performed. All electrochemical tests have been performed in aerated solutions at 308 K. The EIS experiments were conducted in the frequency range with high limit of 100 kHz and different low limit 0.1 Hz at open circuit potential, with 10 points per decade, at the rest potential, after 30 min of acid immersion, by applying 10 mV ac voltage peak-to-peak. Nyquist plots were made from these experiments. The best semicircle can be fit through the data points in the Nyquist plot using a non-linear least square fit so as to give the intersections with the x-axis.
The inhibition efficiency of the inhibitor was calculated from the charge transfer resistance values using the following equation:

$$\mathrm{E\%} = \frac{R_{ct} - R^{\circ}_{ct}}{R_{ct}} \mathrm{x100} \qquad \mathbf{(3)}$$

Where, R°_{ct} and R_{ct} are the charge transfer resistance in absence and in presence of inhibitor, respectively.

2.3. Quantum chemical calculations

Quantum chemical calculations are used to correlate experimental data for inhibitors obtained from different techniques (viz., electrochemical and weight loss) and their structural and electronic properties. According to Koopman's theorem [19], E_{HOMO} and E_{LUMO} of the inhibitor molecule are related to the ionization potential (I) and the electron affinity (A), respectively. The ionization potential and the electron affinity are defined as $I = -E_{HOMO}$ and $A = -E_{LUMO}$, respectively. Then absolute electronegativity (χ) and global hardness (η) of the inhibitor molecule are approximated as follows [20]:

$$\chi = \frac{I+A}{2}\ ,\quad \chi = -\frac{1}{2}(E_{HOMO} + E_{LUMO}) \qquad \mathbf{(4)}$$

$$\eta = \frac{I-A}{2}\ ,\quad \eta = -\frac{1}{2}(E_{HOMO} - E_{LUMO}) \qquad \mathbf{(5)}$$

Where $I = -E_{HOMO}$ and $A = -E_{LUMO}$ are the ionization potential and electron affinity respectively.
The fraction of transferred electrons ΔN was calculated according to Pearson theory [21]. This parameter evaluates the electronic flow in a reaction of two systems with different electronegativities, in particular case; a metallic surface (Fe) and an inhibitor molecule. ΔN is given as follows:

$$\Delta N = \frac{\chi_{Fe} - \chi_{inh}}{2(\eta_{Fe} + \eta_{inh})} \qquad \mathbf{(6)}$$

Where χFe and χinh denote the absolute electronegativity of an iron atom (Fe) and the inhibitor molecule, respectively; ηFe and ηinh denote the absolute hardness of Fe atom and the inhibitor molecule, respectively. In

order to apply the eq. 6 in the present study, a theoretical value for the electronegativity of bulk iron was used $\chi Fe = 7$ eV and a global hardness of $\eta Fe = 0$, by assuming that for a metallic bulk I = A because they are softer than the neutral metallic atoms [21].

The electrophilicity has been introduced by Sastri et al. [22], is a descriptor of reactivity that allows a quantitative classification of the global electrophilic nature of a compound within a relative scale. They have proposed the ω as a measure of energy lowering owing to maximal electron flow between donor and acceptor and ω is defined as follows.

$$\omega = \frac{\chi^2}{2\eta} \quad \textbf{(7)}$$

The Softness σ is defined as the inverse of the η [23]

$$\sigma = \frac{1}{\eta} \quad \textbf{(8)}$$

Using left and right derivatives with respect to the number of electrons, electrophilic and nucleophilic Fukui functions for a site k in a molecule can be defined [24].

$$f_k^+ = P_k(N+1) - P_k(N) \quad for\ nucleophilic\ attack \quad \textbf{(9)}$$

$$f_k^- = P_k(N) - P_k(N-1) \quad for\ electrphilic\ attack \quad \textbf{(10)}$$

$$f_k^+ = [P_k(N+1) - P_k(N-1)]/2 \quad for\ radical\ attack \quad \textbf{(11)}$$

where, $P_k(N)$, $P_k(N+1)$ and $P_k(N-1)$ are the natural populations for the atom k in the neutral, anionic and cationic species respectively.

3. Results and Discussion

3.1. Weight loss measurements

3.1.1. Effect of inhibitor concentration

The weight loss experiments were carried out in a glass cell in 1.0 M HCl with the absence and presence of different concentration of the P2 (10^{-6}-10^{-3}M) at 308K for 6 h imersion. Table 1 summerizes the values of corrosion rate (*v*), surface coverage (θ) and inhibition efficiency *Ew(%),* obtained form gravimetric method. Table 1 suggests that, the increase in inhibitor concentration in the aggressive solution decreases the corrosion rate of mild steel efficiently, while the surface coverage and inhibition efficiency increases. The decrease in weight loss (i.e *v*) with the increase of the P2 inhibitor indicates that the corrosion inhibition process occurs due to the adsorption of the inhibitor molecules on the metal surface [25].

Table 1: Impedance parameters with corresponding inhibition efficiency for the corrosion of mild steel in 1.0 M HCl at different concentrations of (**P2**).

Inhibitor	**Concentration** (M)	***v*** ($mg.cm^{-2}\ h^{-1}$)	$\mathbf{E_w}$ (%)
1M HCl	**--**	0.82	--
P2	$\mathbf{10^{-6}}$	0.42	49
	$\mathbf{10^{-5}}$	0.31	62
	$\mathbf{10^{-4}}$	0.15	82
	$\mathbf{10^{-3}}$	0.08	90

3.1.2. Adsorption isotherm and thermodynamic activation parameters

The dependence of the fraction of report C/q as function of the concentration (C) of P2 was graphically fitted. Figure 1 shows the dependence of the C/θ as function of the concentration of P2.

As can be seen from figure 1 adsorption of P2 obeys the Longmuir isotherm given by equation

$$\frac{\theta}{1-\theta} = C_{inh} \cdot K_{ads} \quad \textbf{(12)}$$

Where K_{ads} is the equilibrium constant of adsorption adsorption/desorption process, θ is Surface covered and C is the inhibitor concentration.
The adsorption of organic compounds on metal surface is explained by the substitution of water molecules which facilitate the access of hydrogen ions to the surface and then the corrosion attack. This replacement may cover the metal surface and then reduces the surface area that is available for the attack of the aggressive ion from the acid solution. The corrosion rate decreases with increase with the inhibitor concentration.

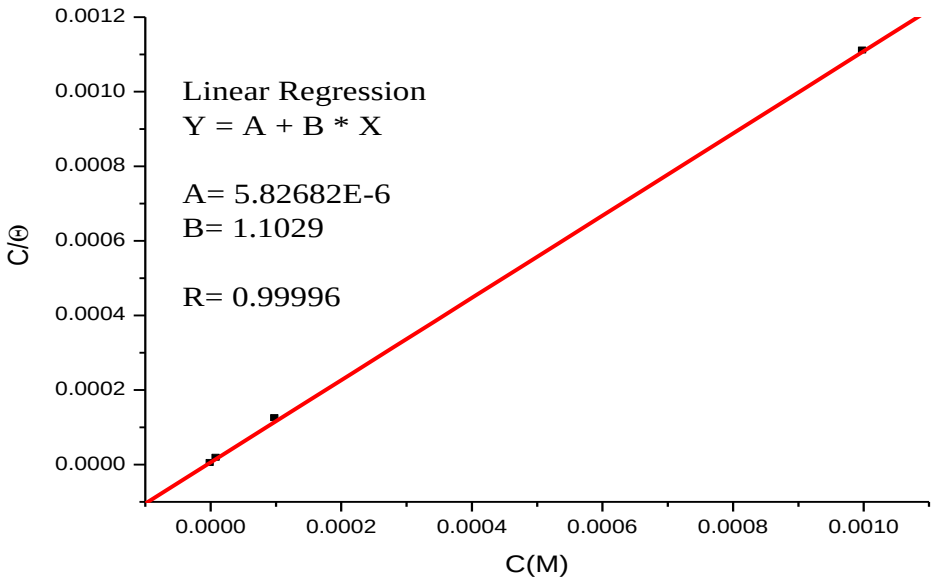

Figure 1: Langmuir isotherm for the adsorption of P2 on the mild steel surface.

As shown in Figure 1, straight lines are obtained, when C/θ is plotted against C and the linear correlation coefficient of the fitted data is good (>0.999). This result corroborates that the inhibition is due to the adsorption of the inhibitors onto the metal surface and the adsorption obeys the Langmuir isotherm.
Based on the Langmuir isotherm, the standard free energy of adsorption ($\Delta G°_{ads}$) can be estimated by the following equation:

$$\Delta G_{ads} = -RT\ln(55{,}5K) \quad \textbf{(13)}$$

Where R is the universal gas constant and T is the absolute temperature.
The calculated value of $\Delta G°_{ads}$ is negative (-41.13 kj/mol). The increasingly negative adsorption free energy ($\Delta G°_{ads}$) reflects the spontaneity of the adsorption of the inhibitor molecules and more $\Delta G°_{ads}$ is negative and more the adsorbed layer on steel surface is stable.
The negative values of $\Delta G°_{ads}$ equal -20 kJ/mol or lower are attributed to the electrostatic interaction between the charged molecules and the charged metal (physisorption). Furthermore, those around -40 kJ/mol or higher involve charge sharing or transfer from organic molecules to the metal surface to form a coordinate type of bond (chemisorption) [26], while values between -20 kJ/mol and -40 kJ/mol indicate both physisorption and chemisorption
[27]. The value of -40 kJ/mol is usually adopted as a threshold value between chemi- and physisorption [28].
The values of $\Delta G°_{ads}$ for these Schiff bases point to the spontaneity of the adsorption process under investigated experimental conditions, and it also points out the adsorption of compounds occurs predominantly by chimical adsorption [29].

3.2. Electrochemical impedance spectroscopy (EIS)

The Nyquist plots on mild steel in the presence and absence of various concentration of P2 in 1 M HCl are given in Figure 2.

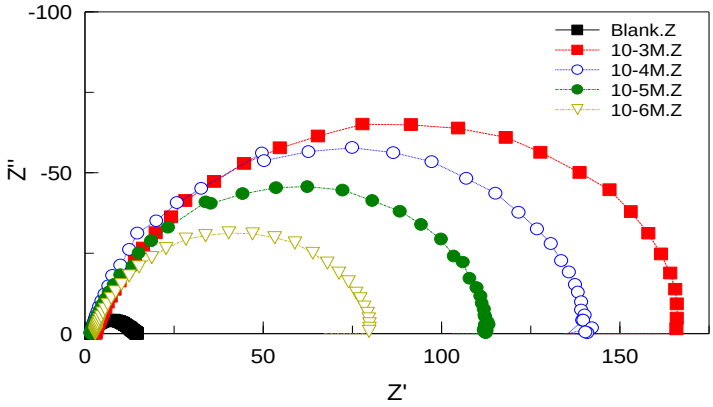

Figure 2: Nyquist diagram for mild steel in 1 M HCl in the absence and presence of P2.

It can be seen clearly from Figure 2, that the Nyquist plot shows an apparent increase in the total impedance with the increase of the inhibitor concentration. Figure 2 shows that the increase in inhibitor concentration increases the diameter of the depressed semi circle, which may be attributed to the adsorption of the P2 inhibitor on the mild steel surface.
The increased surface smoothness is further supported by increased values of phase angle in the presence of inhibitors as reflected in the Bode plots (Figure 3) and Table 2. The increased values of the slopes of the linear portion of the Bode impedance modulus plots at intermediate frequencies further support the formation of protective film of inhibitor molecules on the steel surface.

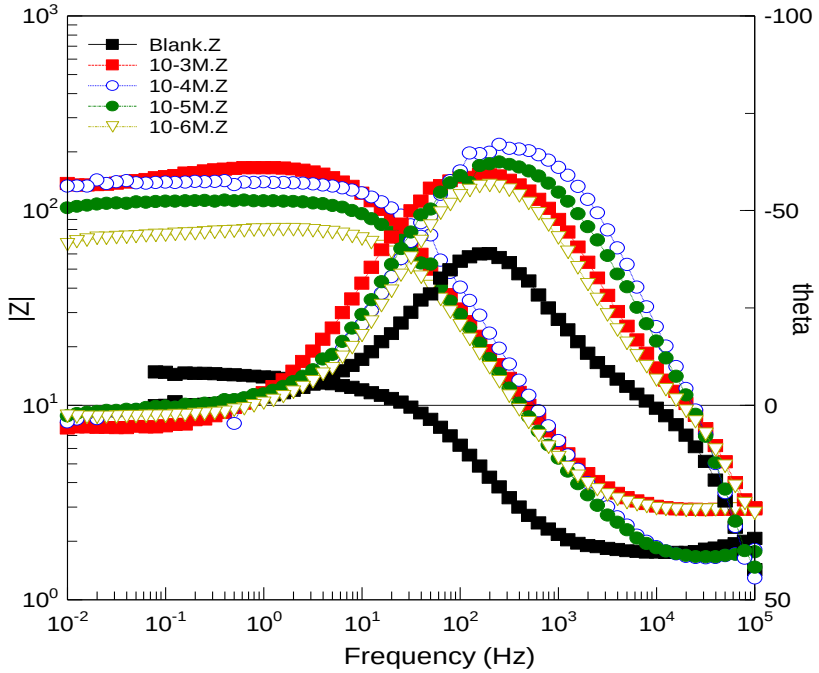

Figure 3: Bode and phase plots of mild steel in 1.0 M HCl and in the presence different concentrations of P2 at 308 K.

The values are tabulated in Table 2, which suggest that Rt increases and *C*dl tends to decrease when the concentration of inhibitor increases. A decrease in the C_{dl} values, which can result from a decrease in the local dielectric constant and/or an increase in the thickness of the electrical double layer, suggests that the P2 function by adsorption at the metal solution/interface [30].
The increase of Rct is attributed to the adsorption of the inhibitor molecules on the mild steel/HCl interface, which decrease the corrosion rate of the mild steel surface.

Table 2: Electrochemical parameters for mild steel in 1 M HCl without and with different concentrations of **(**P2**)** at 308K.

Concentration (M) / Prameters	**1M HCl**	**10^{-6}**	**10^{-5}**	**10^{-4}**	**10^{-3}**
Real Center	9.25	39.768	56.776	70.713	79.379
Imag. Center	1.62	3.3906	8.3805	10.68	2.0977
Diameter	15.13	72.671	110.07	138.94	147.35
Deviation	0.15	2.5766	2.0693	1.8954	8.052
Low Intercept R_s ($\Omega.cm^2$)	1.86	3.591	2.3823	2.0666	5.7325
High Intercept R_t ($\Omega.cm^2$)	16.64	75.945	111.17	139.36	153.02
Depression Angle	12.42	5.3542	8.7588	8.8432	1.6315
ω_{max} (rad s^{-1})	929.60	203	145.01	170.44	96.61
Estimated R_t($\Omega.cm^2$)	14.78	72.354	108.79	137.29	147.29
Estimated C_{dl}($F.cm^{-2}$)	7.11 E-5	6.7787E-5	6.2652E-5	4.2226E-5	7.0246E-5
E_R(%)	--	80	86	89	**90**

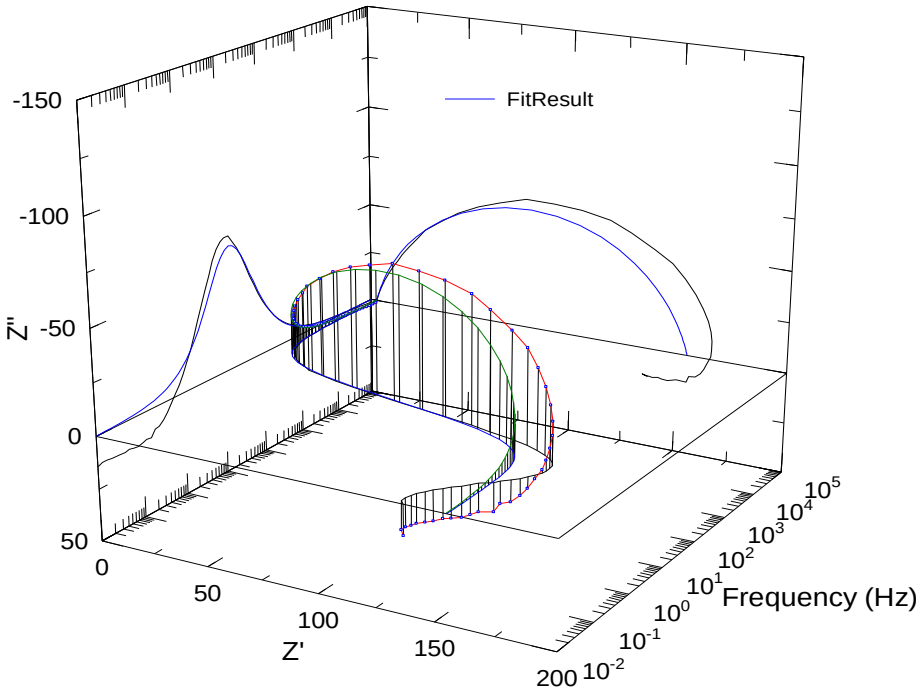

Figure 4: EIS Nyquist and Bode diagrams 3D for mild steel/1 M HCl + 10^{-3} M of **P2** interface: (------) experimental; (------) fitted data.

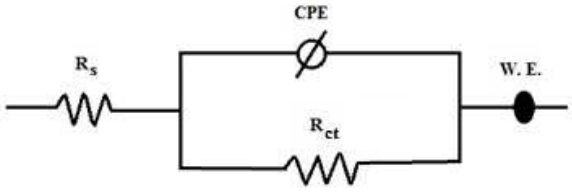

Figure 5: Equivalent circuit model used to fit the impedance spectra.

Figure 5 shows the electrical equivalent circuit diagram to model mild steel/HCl interface which consists of a constant phase element (CPE), charge transfer resistance (Rct) and solution resistance (Rs). In general, the CPE is required for the distribution of the relaxation time, as a result of surface inhomogenities [31].

3.3. Computational theoretical studies

The FMOs (HOMO and LUMO) are very important for describing chemical reactivity. The HOMO containing electrons, represents the ability (E_{HOMO}) to donate an electron, whereas, LUMO haven't not electrons, as an electron acceptor represents the ability (E_{LUMO}) to obtain an electron. The energy gap between HOMO and LUMO determines the kinetic stability, chemical reactivity, optical polarizability and chemical hardness–softness of a compound [32].
Firstly, in this study, we calculated the HOMO and LUMO orbital energies by using B3LYP method with 6-31G which is implemented in Gaussian 09 packadge [33-34]. All other calculations were performed using the results with some assumptions. The higher values of E_{HOMO} indicate an increase for the electron donor and this means a better inhibitory activity with increasing adsorption of the inhibitor on a metal surface, whereas E_{LUMO} indicates the ability to accept electron of the molecule. The adsorption ability of the inhibitor to the metal surface increases with increasing of E_{HOMO} and decreasing of E_{LUMO}. The HOMO and LUMO orbital energies of the P2 inhibitors were performed and were shown in Table 3 and Figure 6. High ionization energy (> 6 eV) indicates high stability of P2 inhibitor [35], the number of electrons transferred (ΔN), dipole moment, Ionization potential**,** electron affinity, electronegativity, hardness, Softness and total energy were also calculated and tabulated in Table 3.

Table 3: Quantum chemical parameters for P2 obtained in gas and aqueous phase with the DFT at the B3LYP/6-31G level.

Prameters	Gas phase	Aqueous phase
Total Energy *TE* (eV)	-28945.9	-28946.4
E_{HOMO} (eV)	-6.9405	-6.3764
E_{LUMO} (eV)	-1.1064	-2.7433
Gap ΔE (eV)	5.8341	3.6331
Dipole moment μ (Debye)	4.4908	5.2826
Ionization potential I (eV)	6.9405	6.3764
Electron affinity A	1.1064	2.7433
Electronegativity χ	4.0234	4.5599
Hardness η	2.9170	1.8165
Electrophilicity index ω	2.7747	5.7230
Softness σ	0.3428	0.5505
Fractions of electron transferred ΔN	0.5102	0.6716

The value of ΔN (number of electrons transferred) show that the inhibition efficiency resulting from electron donation agrees with Lukovit's study [36]. If $\Delta N < 3.6$, the inhibition efficiency increases by increasing electron donation ability of these inhibitors to donate electrons to the metal surface [37].
Pertinent valence and dihedral angles, in degree, of the studied inhibitor calculated at B3LYP/6-31G(d,p) in gas and aqueous phases are given in the table 4.
Table 5 displays the most relevant values of the natural population (P(N), P(N-1) and P(N+1)) with the corresponding values of the Fukui functions (f_k^+, f_k^- and f_k^0) of the studied inhibitors. The calculated values of the f_k^+ for inhibitors are mostly localized on the isatine ring, namely C_4, C_7, O_{13} and O_{14}, indicating that the isatine ring will probably be the favorite site for nucleophilic attacks.

Table 4: Pertinent valence and dihedral angles, in degree, of the studied inhibitors calculated at B3LYP/6-31G(d,p) in gas, G and aqueous, A phases

Angle	phase	Value (°)
[$O_{14}C_8N_{15}$]	G	127.24
	A	127.23
[$C_{28}C_{22}N_{27}$]	G	112.92
	A	112.92
[$O_{14}C_8N_{15}C_{16}$]	G	1.74
	A	1.24
[$C_{28}C_{22}N_{27}C_{20}$]	G	66.84
	A	70.76

Table 5: Pertinent natural populations and Fukui functions of P2 calculated at B3LYP/6-31G in gas (G) and aqueous phases.

	Phase	*P(K)*	*P(K+1)*	*P(K-1)*	*f*	f^+	f^0
C4	G	6,1911	6,2803	6,1738	0,0891	0,0173	0,0533
	A	6,1808	6,2845	6,0822	0,1038	0,0986	0,1012
C7	G	5,5590	5,7324	5,5296	0,1734	0,0294	0,1014
	A	5,4991	5,6938	5,5171	0,1948	-0,0180	0,0884
O13	G	8,4651	8,6344	8,4138	0,1693	0,0513	0,1103
	A	8,5235	8,6959	8,4334	0,1724	0,0901	0,1313
O14	G	8,4976	8,6783	8,4566	0,1808	0,0410	0,1109
	A	8,5872	8,7037	8,4730	0,1165	0,1142	0,1153

The geometry of P2 in gas and aqueous phase (Figure 6) were fully optimized using DFT based on Beck's three parameter exchange functional and Lee–Yang–Parr nonlocal correlation functional (B3LYP) [38-40] and the 6–31G. The optimized structure shows that the molecule P2 has a non-planar structure. The HOMO and LUMO electrons density distributions of **P2** are given in Table 4.

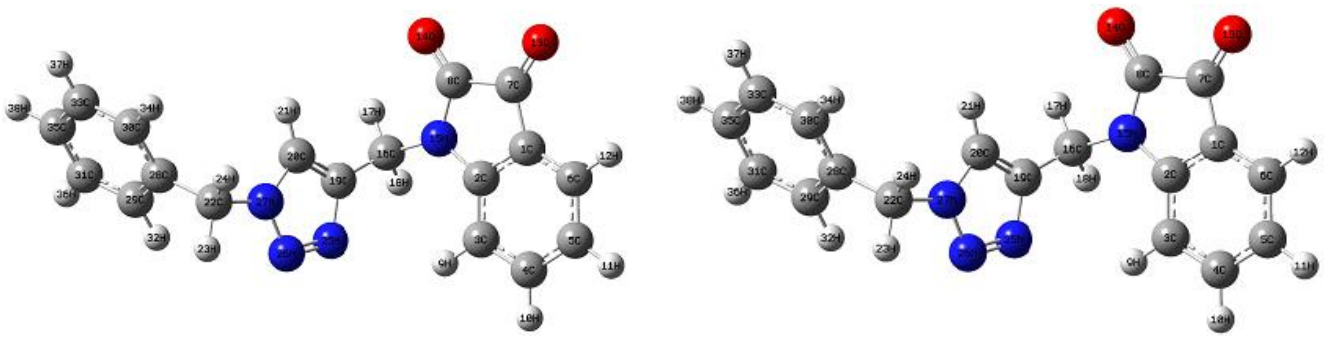

Gas phase Aqueous phase

Figure 6: Optimized molecular structures in gas and aqueous phase with the DFT at the B3LYP/6-31G level

As we know, frontier orbital theory is useful in predicting the adsorption centres of the inhibitors responsible for the interaction with surface metal atoms. Table 6 shows the HOMO and LUMO orbital contributions for the neutral studied inhibitor. The HOMO densities were concentrated on isatine ring.

Table 6: The HOMO and the LUMO electrons density distributions of P2 in gas and aqueous phase computed at B3LYP/6-31G level for neutral forms.

	Gas	Aqueous
HOMO	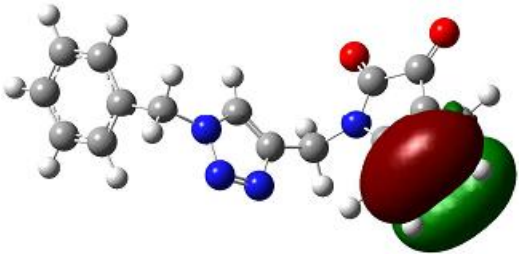	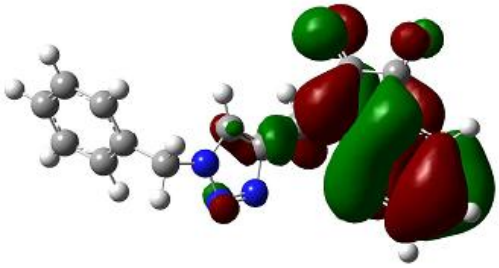
LUMO	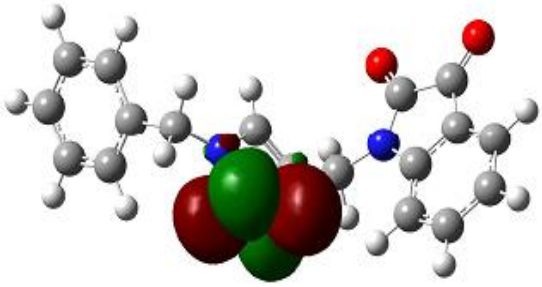	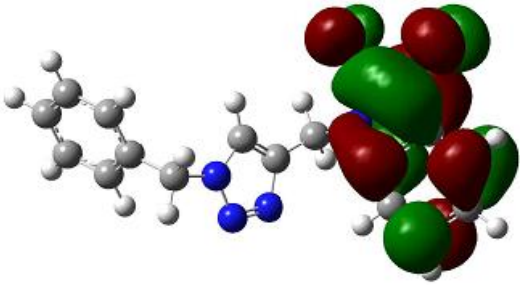

Conclusion

From the overall experimental results the following conclusions can be deduced:

- The inhibition efficiency increases with increasing of inhibitor concentration to attain a maximum value of 90 % for inhibitor P2 at 10^{-3} M.
- The synthesized molecules adsorb on the steel surface according to the Langmuir isotherm.
- Double-layer capacitances decrease with respect to blank solution when the synthesized inhibitor is added.
- Quantum chemical calculations provided more detailed accounts of how different electron donating and accepting substituents tuned the extent and mode of the donor-acceptor interactions between the metal and the inhibitor molecules.

Reference

1. Abele E., Abele R., Dzenibs O., *Chemistry of Hetrocylic Compounds.* 39 (2003) 1.
2. Mesropyan E. G., Ambrtsumyan G. B., Avetisyan A. A., *Russian Journal Org. Chem*. 39(8) (2003) 1130.
3. Zemtsova M. N., Trakhtenborg P. L., *Russian Journal Org. Chem*. 38 (2003) 1803.
4. Tatsungi J., Ikuma K., Izawa Y., Tetrahedron Lett. 36 (1995) 8611.
5. Elderfield R., *Heterocyclic Compounds.* 3 (1954) 164.
6. Elderfield R., *Heterocyclic Compounds*. 4 (1955) 36.
7. Garden S. J., Torres J. C., Ferreira A. A., Silva R. B., Pinto A. C., *Tetrahedron Lett.* 38 (1977) 1501.
8. Tatsungi J., Izawa Y., *Synth. Commun*. 28(1988)859.
9. Traynelis V. J., Hergenvother W. C., *J. Org. Chem*. 29 (1964) 221.
10. Traynelis V. J., Hergenvother W. C., *J. Org. Chem. Soc*. 86 (1964) 298.
11. Gassmen P. G., Cue J. B. W., Luth T.Y., *J. Org. Chem*. 42 (1977) 1344.
12. Ujiie T., *Chem. Pharm. Bull*. 14 (1966) 461.
13. Pfitzinger W., *J. Prakt. Chem*. 33(2) (1886) 100.
14. Popp F. D., *Adv. Heterocycl. Chem*. 18 (1975) 2.
15. Joaquime F. M. da Silva, Simon J .Garden, Angelo C. Pinto, *Journal of the Brazilian Chemical Society*. 12(3) (2001) 273-324.
16. Garden S. J., Torres J. C., Ferreira A. A., Silva R. B., Pinto A. C., *Tetrahedron Lett.* 38 (1977) 1501.
17. Tatsungi J., Hara T., Izawa Y., *Chem. Let*. (1977) 177.

18. Qachchachi F. Z., Kandri Rodi Y., Essassi E. M., Bodensteiner M. and El Ammari L., *Acta Cryst*. E70 (2014) o588.
19. Pearson R.G., *Inorg. Chem*. 27 (1988) 734–740.
20. Sastri V.S., Perumareddi J.R., *Corrosion*. 53 (1997) 617–622.
21. Pearson R.G., *Inorg. Chem*. 27(1988)734.
22. Sastri, V. and Perumareddi S., *J.R., Corrosion*. 53 (1997) 671.
23. Udhayakala P., Rajendiran T. V., and Gunasekaran S., *Journal of Chemical, Biological and Physical Sciences A*. 2 (2012) 1151-1165.
24. Roy R.K., Pal S., Hirao K., *J. Chem. Phys*. 110(1999)8236.
25. Elmsellem H., Basbas N., Chetouani A., Aouniti A., Radi S., Messali M., Hammouti B., Portugaliae. Electrochimica. Acta. 2(2014)77.
26. Elouali, I., Hammouti, B., Aouniti, A., Ramli, Y., Azougagh, M., Essassi, E.M., Bouachrine M. *J. Mater. Environ.Sci.* 1 (2010) 1.
27. Kustu C., Emregul K.C., Atakol O., *Corros. Sci*. 49 (2007) 2800.
28. Singh A K., Quraishi M.A. *J. Mater. Environ. Sci.* 1 (2010) 101.
29. Elmsellem H., Nacer H., Halaimia F., Aouniti A., Lakehal I., Chetouani A., Al-Deyab S. S., Warad I., Touzani R., Hammouti B, Int. J. Electrochem. Sci. 9 (2014) 5328.
30. Elmsellem H., AounitiA., Youssoufi M.H., BendahaH., Ben hadda T., Chetouani A., Warad I., Hammouti B., *Phys. Chem. News*. 70 (2013) 84.
31. Elmsellem H., Harit T., AounitiA., Malek F., Riahi A., Chetouani A., Hammouti B., *Protection of Metals and Physical. Chemistry of Surfaces*. 5 (2015) 873.
32. Govindarajan M., Karabacak M., *Spectrochim Acta Part A Mol Biomol Spectrosc*, 85 (2012)251-60.
33. Becke A.D., *J. Chem. Phys*. 98 (1993) 1372.
34. Filali Baba Y., Elmsellem H., Kandri Rodi Y., Steli H., AD C., Ouzidan Y., Ouazzani Chahdi F., Sebbar N. K., Essassi E. M., and Hammouti B., *Der Pharma Chemica*. 8 (2016) 159-169.
35. Elmsellem H., Karrouchi K., Aouniti A., Hammouti B., Radi S., Taoufik J., Ansar M., Dahmani M., Steli H. and El Mahi B., *Der Pharma Chemica*. 7 (2015) 237-245.
36. Lukovits I., Kalman E., Zucchi F., *Corrosion*. 57 (2001) 3-7.
37. Sikine M., Kandri Rodi Y., Elmsellem H., Krim O., Steli H., Ouzidan Y., Kandri Rodi A., Ouazzani Chahdi F., Sebbar N. K., Essassi E. M., *J. Mater. Environ. Sci*. 7 (2016) 1386-1395.
38. Hjouji M. Y., Djedid M., Elmsellem H., Kandri Rodi Y., Ouzidan Y., Ouazzani Chahdi F., Sebbar N. K., Essassi E. M., Abdel-Rahman I., Hammouti B., *J. Mater. Environ. Sci*. 7 (2016) 1425-1435.
39. Lee C., Yang W., Parr R.G., *Phys. Rev*. B. 37 (1988) 785.
40. Chakib I., Elmsellem H., Sebbar N. K., Lahmidi S., Nadeem A., Essassi E. M., Ouzidan Y., Abdel-Rahman I., Bentiss F., Hammouti B., *J. Mater. Environ. Sci*. 7 (2016) 1866-1881.